

Multi-Criteria Ranking of Z-Source Inverter Topologies for a Three-Wheel Fuel Cell Hybrid Electric Vehicle

Thang V. Do, *Student Member, IEEE*, Mohsen Kandidayeni, *Member, IEEE*, João Pedro F. Trovão, *Senior Member, IEEE*, Loïc Boulon, *Senior Member, IEEE*

Abstract—Replacing the regular two-stage inverters with a Z-source inverter (ZSI), based on single conversion, has come under attention in fuel cell (FC) hybrid electric vehicles (HEVs). This substitution is to decrease the circuit complexity, cost, and required space. However, fulfilling these goals highly depends on the selection of a suitable topology. This paper performs a multi-criteria ranking to deeply analyze the impact of different ZSI topologies on the performance of a recreational FC-HEV, composed of FC stack and lithium-ion capacitor bank. First, the dual-energy sources are embedded into the Z-source network (ZSN). Subsequently, the Preference Ranking Organization METHod for Enrichment Evaluation (PROMETHEE) is utilized to rank different possible ZSI topologies based on four scenarios (standard, compactness, input current ripple, and compactness versus input current ripple). This analysis indicates that each scenario can have a suitable topology with respect to its requirements. Finally, the two highest-ranked ZSI topologies according to standard scenario are implemented by signal hardware-in-the-loop (HIL) to validate the effectiveness of the performed analysis. The results indicate that the use of the ZSI topologies lead to higher average efficiencies (1.98% and 4.07%), and smaller size and volume of passive components, compared to a conventional two-stage inverter.

Index Terms— Fuel-cell electric vehicle (FCEV), Multi-criteria decision-making, PROMETHEE, Z-source inverter topologies.

I. INTRODUCTION

Hybridization with an energy storage system (ESS) through power electronic converters is vital in fuel cell hybrid electric vehicle (FC-HEVs). In this regard, conventional two-stage inverters, comprising dc-dc converters and inverters, are frequently used in these vehicles [1], [2]. However, they operate with high-voltage stresses, large conduction losses, poor reliability, and deadtime requirements owing to their long duty

Manuscript submitted May 25, 2022; revised xxx, 2022; accepted xxx, 2022. Date of publication xxx, 2022; date of current version xxx, 2022. This work is supported in part by Grants 950-230672 from Canada Research Chairs Program and in part by Grants RGPIN-2017-05924 and RGPIN-2018-06527 from the Natural Sciences and Engineering Research Council of Canada.

Thang V. Do is with the Department of Electrical Engineering and Computer Engineering, University of Sherbrooke, Sherbrooke, QC, J1K 2R1, Canada, (e-mail: Thang.Do.Van.Thang@USherbrooke.ca).

Mohsen Kandidayeni is with the electric-Transport, Energy Storage and Conversion Lab (e-TESE), Department of Electrical Engineering and Computer Engineering, University of Sherbrooke, Sherbrooke, QC J1K 2R1, Canada, and also with the Hydrogen Research Institute (IRH), Université du Québec à Trois-Rivières, Trois-Rivières, QC G8Z 4M3, Canada (e-mail: mohsen.kandidayeni@usherbrooke.ca).

João Pedro F. Trovão is with the Department of Electrical Engineering and Computer Engineering, University of Sherbrooke, Sherbrooke, QC, J1K 2R1, Canada, and also with Polytechnic of Coimbra (IPC-ISEC) and INESC Coimbra, Portugal (e-mail: Joao.Trova@USherbrooke.ca).

Loïc Boulon is with the Hydrogen Research Institute, University of Québec at Trois-Rivières, Trois-Rivières, QC G9A 5H7, Canada, (e-mails: Loic.Boulon@uqtr.ca).

cycles. Therefore, these inverters not only lead to high circuit complexity and cost but also require large space and achieve low efficiency in FC-HEVs.

To overcome the weaknesses of the two-stage inverters, the use of new single-stage converters has come under attention. For instance, Z-Source inverter (ZSI) and quasi-ZSI (q-ZSI) have been widely utilized to replace the traditional one in the distributed generation systems [3]. In fact, many ZSI topologies have been proposed to increase the voltage gains and decrease the voltage and current stresses on the components at a lower shoot-through duty cycle for the conventional ZSI and q-ZSI. These topologies can be mainly categorized into coupled and non-coupled inductor/transformer. The coupled topologies might lead to unwanted voltage spikes because of the existing leakage inductances and electromagnetic interference (EMI) noise problems [4]. By applying snubber circuits, the effects of the leakage inductance can be reduced while decreasing the voltage gain and increasing the cost of the topologies. On the other hand, the non-coupled topologies are commonly developed by adding more active and passive components to modify the ZSN [5]. However, they still have limitations to be utilized with broad range loads like FC-HEV applications. These topologies can operate under the discontinuous conduction mode at the light load or small inductance values in ZSN designs. This results in uncontrollable voltage drop at the dc-link. These issues can be solved by selecting a suitable topology, in which the diode can be added by the an anti-parallel power switch for bidirectional power flow, such as bidirectional q-ZSI (Bq-ZSI) [6], revised active-switched-capacitor/inductor (ASC/L) q-ZSI [7], active switched (AS) q-ZSI [8], active-switched-capacitor/switched-inductor (ASC/SL) q-ZSI [9], switched-inductor (SL) q-ZSI [10], cSL-qZSI and rSL-qZSI [11], diode assisted (DA) q-ZSI, and capacitor-assisted (CA) q-ZSI [12].

Recently, many research areas of ZSI topologies with dual-sources have been investigated for electric vehicle (EV) applications. The traditional ZSIs and qZSIs have been utilized to couple the ESSs into their ZSN without adding more dc-dc [13]–[15]. By integrating the batteries (BATs) in parallel with one capacitor of the ZSNs, these converters enable to not only increase the efficiency but also remarkably decrease the system size and cost in EVs [13], [14]. The robustness of the FC-HEV against power variations is increased by embedding the BAT into the ZSN of the ZSI [15]. Regarding the control method and energy management strategy (EMS) of these dual-source

topologies, a fractional-order PI controller and a fuzzy controller are employed to enhance the dynamic performance of the BAT current control in the HESS Bq-ZSIs in [16], [17]. Frequency diving coordinated controls are investigated to satisfy the demand of the dynamic responses and obtain optimal performance in terms of the dynamic power regulation and the BAT current stress [13], [14]. Moreover, understanding the dynamic characteristics of the HESS qZSI topologies is necessary for their adoption in various applications [18]. However, there is a lack of study regarding a systematic procedure to rank the dual-source Z-source topologies for improving the performance of FC-HEVs. To fill this gap, this paper proposes a systematic methodology to rank the best ZSI topologies.

Choosing an appropriate ZSI topology in a FC-HEV is

TABLE I
COMMON A MULTI-CRITERIA DECISION-MAKING (MCDM) METHODS WITH THEIR PROS AND CONS.

MCDM methods	Approaches	Advantages	Disadvantages
Utility theory-based approaches	Analytical hierarchy process (AHP)	- Based on a hierarchical structure; thus, better focusing on each criterion employed in the evaluations. - Doesn't involve complicated mathematics.	- Interdependence between alternatives and objectives can result in an inaccurate result. - Important information might be lost due to the used additive aggregation. - Requires data collected based on experience.
	Technique for Order Preference by Similarity to Ideal Solutions (TOPSIS)	- Operates with fundamental ranking. - The information is not independent.	- This method is implemented on the basis of Euclidean distance and thus the difference between negative and positive values is not considered. - The value of the attributes should be monotonous (rising or falling).
	Multicriteria Optimization and Compromise Solution (VIKOR)	- An updated version of TOPSIS. - Calculate the ratio of positive and negative ideal solutions thus eliminating the impact.	- Difficult to obtain reliable results when having conflicting situations.
Outranking-based approaches	PROMETHEE	- It operates with qualitative and quantitative information. - Be implemented based on its solid mathematical basis, thus giving more accuracy in results. - Straightforward to apply.	- Depending on the decision maker to designate weight gains. - Complicated and thus users are restricted to experts.
	Elimination and Choice Translating Reality (ELECTRE)	- It pays attention to uncertainty.	- Requests more parameters with a more monotonous calculation process and less transparent results.

extremely crucial to increase the performance, and decrease the system size and volume. In this regard, utilizing a MCDM approach seems to be necessary as multiple objectives involve in this problem. MCDM methods are mainly divided into two groups of utility theory and outranking as presented in TABLE I. Many MCDM methods have lately been employed in the EV application. Regarding the utility theory-based approaches, a hybrid AHP-TOPSIS approach is employed to select the suitable electric bus in the center of Ankara [19]. VIKOR and TOPSIS methods are also utilized to figure out the best vehicle engine system in [20]. However, the total scores of these approaches are calculated by aggregation operators which are based on utilizing utility functions for different criteria. Therefore, these scores may lead to unreliable results in FC-HEV power electronic converters in which various criteria, such as efficiency, cost, size, and volume, could be conflicted or combined. Concerning the outranking-based approaches, PROMETHEE methods are highly straightforward compared to other methods like ELECTRE. This is due to requiring fewer parameters from decision-makers (DMs). Furthermore, they are implemented based on their solid mathematical principle. The effectiveness of PROMETHEE has been already proven in EV application. For instance, it is utilized to select the types of the EV employed in urban transport and the suitable location for EV charging stations in [21], [22], respectively. As a result, this method is used in this study for supporting the analysis regarding the topology selection.

In light of the above-discussed matters, this paper employs PROMETHEE for multi-criteria ranking of different ZSI topologies in a recreational FC-HEV. Hence, beyond the theoretical study, this paper is built around an application case. The recreational three-wheel FC-HEV has been studied in [23]. This vehicle employs the traditional two-stage inverter, which not only suffers from low performance but also enhances the requirements of the cost and space. Thus, the selection of a suitable ZSI topology to replace the traditional one can result in superior performance and lower system weight and volume. This work is an extension of the paper in [16], where we presented approaches to lower down the system size and volume and to enhance the efficiency for EV-based power electronics systems.

The major contributions of this paper are as follows:

- Presenting a multi-criteria hybridization considering the high specific-energy (HSE) source, FC, and a high specific-power (HSP) source, li-ion capacitor (LiC), for an FC-HEV.
- Proposing a framework to choose suitable power converters at the system level for an FC-HEV application.

To justify the performed analysis, a signal hardware-in-the-loop (HIL) setup is utilized to provide simulations with microcontroller in the loop for the two highest-ranked topologies compared to the conventional one. In this regard, the computing time of the HIL simulation is shorter than the time step. Moreover, it is a considerable platform for tackling the issues of offline tools, owing to its extremely high security and repeatability. Thus, it is employed to execute the power converters more precisely.

The paper is structured as follows. Section II describes the studied three-wheel electric vehicle configuration along with the schematics of all selected dual-source ZSI. The PROMETHEE ranking analysis is presented in Section III. Results and discussion with the PROMETHEE and HIL validations are shown in Section IV, followed by the conclusion section.

II. METHODOLOGICAL FRAMEWORK

A. Configuration and Specification of the three-wheel FC-HEV

The studied vehicle, as shown in Fig. 1, is a three-wheel EV (e-TESS-3W platform) from University of Sherbrooke. In [23], [24], conventional two-stage inverters are employed in this vehicle. The recent powertrain architecture of the EV under study is shown in Fig. 1.

In order to enhance its performance, the electrical traction drive utilizes hybrid ESS with ZSI topologies. The average power is provided by a FC stack, and LiCs are employed to transfer/store high-frequency power instantaneously in acceleration and braking operations. This system is equipped with a 13kW-100V permanent magnet synchronous motor (PMSM). By embedding the LiCs into the ZSN, the power flow between the PMSM and the FC needs to be controlled, and the rest will be automatically supplied by the LiCs. The fundamental parameters of this vehicle are given in TABLE II.

B. ZSI Topologies with Dual-Source.

Choosing proper ZSI topologies that can perform in a wide-range of loads is really critical in FC-HEVs. Firstly, these topologies need to deal with the bidirectional power flows in order to overcome the uncontrollable dc-link voltage-drops. Secondly, HSP sources should be placed close to the dc-link to provide/restore large amount of regenerative energy. By replacing active switches with the diodes in the original topologies [8]–[12], the proposed high-performance (HP) ZSI topologies for the current manuscript are realized in Fig. 2.

In order to gain data and simplify the multi-criteria analysis, all the ZSI topologies are simulated offline in MATLAB/Simulink™ using the same parameters presented in TABLE II. Moreover, the following conditions are considered:

- The same control algorithm, as shown in Fig. 3, is utilized for all the considered topologies. A simple energy management strategy is employed to determine the required power from the FC.
- Field-oriented control (FOC) is used to control the PMSM following the specific driving cycle.
- The same initial state of charge (SOC) is used for the LiCs, in which the dc-link voltage should be around 100 V. Thus, the same voltage gain is applied to all the ZSI topologies.
- To compare the efficiency of different topologies, the same parameters are used for the components. These efficiencies are average values calculated by simulation results of the same driving cycle (Artemis_short) from time $t = 2.2s$ to $22s$.
- The same inductance values are utilized to easily obtain the FC current ripple among all topologies.

- To evaluate the system size, volume, and cost of the topologies for implementing the PROMETHEE method, the values of passive components are designed again at rated powers with the same voltage and current ripple percentages at 2.5% and 5%, respectively.
- Only 9 qZSI topologies are considered in this work to implement the proposed framework. This is because these converters provide more reliable results than others with better tradeoffs between the efficiencies and the passive components' size and volumes.
- Many qZSI topologies are realized by adding more passive and active components to the ZSN of the conventional ZSI and q-ZSI; however, this might enable them to have higher voltage gains, lower power losses, and smaller current ripples than topologies with fewer components. Thus, they are still considered to carry out the proposed framework.

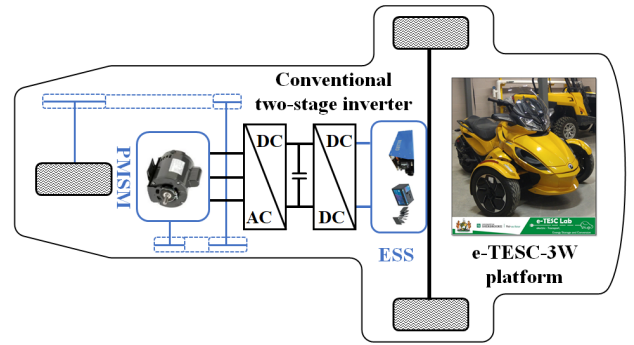


Fig. 1. Studied e-TESS lab three-wheel electric vehicle.

TABLE II
FULL-SCALE SYSTEM PARAMETERS

Parameters	Symbols	Values
Vehicles (e-TESS-3W platform)		
Vehicle mass	m_{eq}	350 kg
Vehicle front area	A_{aero}	1.25 m ²
Wheel radius	r	0.305 m
Belt transmission drive ratio	G_{gb}	5.033 (30:151)
Belt transmission drive efficiency	η_{gb}	95%
Maximum vehicle speed	$V_{EV,max}$	140 km/h
PMSM parameters		
Phase inductance	L_d, L_q	62 - 110 μ H
Rotor inertia	J	0.096 kg. m ²
Internal phase resistance	R_s	0.0027 Ω
Number of pole pairs	ρ	5
Rated power	P_r	13 kW
qZSI topologies and the conventional two-stage inverter parameters		
Inductance	$L_{1-2-3-4}, L_{BC-VSI}$	0.2 - 0.5 mH
DC inductor resistance	$r_{L-1-2-3-4}, r_{L-BC-VSI}$	12.56 - 27.06 m Ω
Capacitance	$C_{1-2-3-4}, C_{BC-VSI}$	2.2 - 2.2 mF
Equivalent series resistance	r_c	21 m Ω
Switching frequency	f_s	10 kHz
On resistance of the switch devices	r_{k0}	9 m Ω
Threshold voltage	v_{k0}	1.45 V
Diode resistance	$r_{F0-1-2-3-4-5-6}$	14 m Ω
Diode forward voltage	$V_{F0-1-2-3-4-5-6}$	1.5 V
Driving cycle	-	Artemis_short
Fuel cell parameters		
Number of cell stacks	N_{FC}	75
Rated power	P_{PF}	14.4 kW
Lithium Ion Capacitor parameters for HIL validation		
Operating voltage range	V_{LiCs}	2.2V-3.8V
Capacitance	C_{LiC}	3300 F
Equivalent series resistance	R_{ESR}	1 m Ω
Number of series cells	$N_{S-ZSI}, N_{S-BC-VSI}$	6 - 36
Number of parallel cells	$N_{P-ZSI}, N_{P-BC-VSI}$	6 - 1

C. Global Methodology

Selecting the best ZSI topologies for the FC-HEV is considered as a MCDM problem. The MCDM method is frequently employed for making preference decisions in applications with restrained solutions as well as a finite group of alternatives.

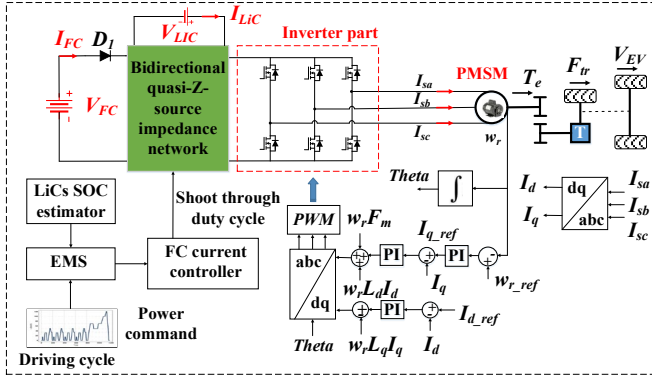


Fig. 3. Control algorithm for the considered ZSI topologies while implementing the PROMETHEE method.

The methodology deals with an analysis framework, as illustrated in Fig. 4, based on MCDM to rank dual-source ZSI topologies in the explained FC-HEV. To this end, the following steps are taken: (i) with respect to the established criteria for the FC-HEV, the suitable ZSI topologies are chosen; (ii) the required data for analysis are obtained according to each criterion using offline simulation on MATLAB/Simulink™; (iii) different scenarios are produced to give a wider scope for the multi-criteria analysis; (iv) visual PROMETHEE software is utilized to rank the ZSI topologies for the proposed scenarios.

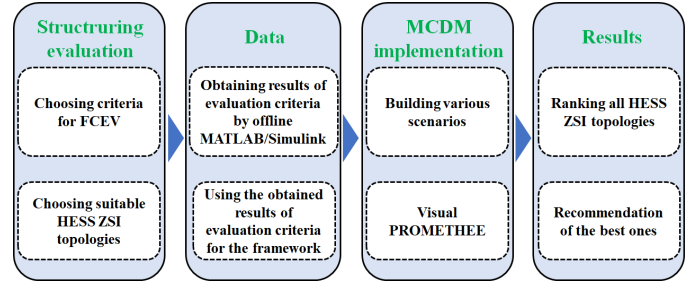


Fig. 4. MCDM process flowchart for the FC-HEV application.

In this study, the PROMETHEE is utilized to identify the best ZSI topologies for the FC-HEV due to its solid mathematical principle [22].

III. PROMETHEE COMPLETE RANKING ANALYSIS

PROMETHEE utilizes the preferential function to show the preference discrepancy between alternative pairs according to each criterion [25]. Then, pairwise comparisons of the alternatives from the results of the preference functions lead to specific outranking relations. While the positive flow gives the advantages of all alternatives, the negative flow expresses their drawbacks. The alternatives are completely ranked from the worst ones to the best ones by the net result of these two flows.

Assuming $A = \{a_1, \dots, a_n\}$ and $G = \{g_1, \dots, g_k\}$ are the groups of alternatives and evaluation criteria, respectively, the procedure of PROMETHEE approach is illustrated in Fig. 5.

A. Define the Multi-Criteria for the FC-HEV

Selecting appropriate low-voltage and high-current ZSI topologies are essential in FC-HEVs due to the electrical

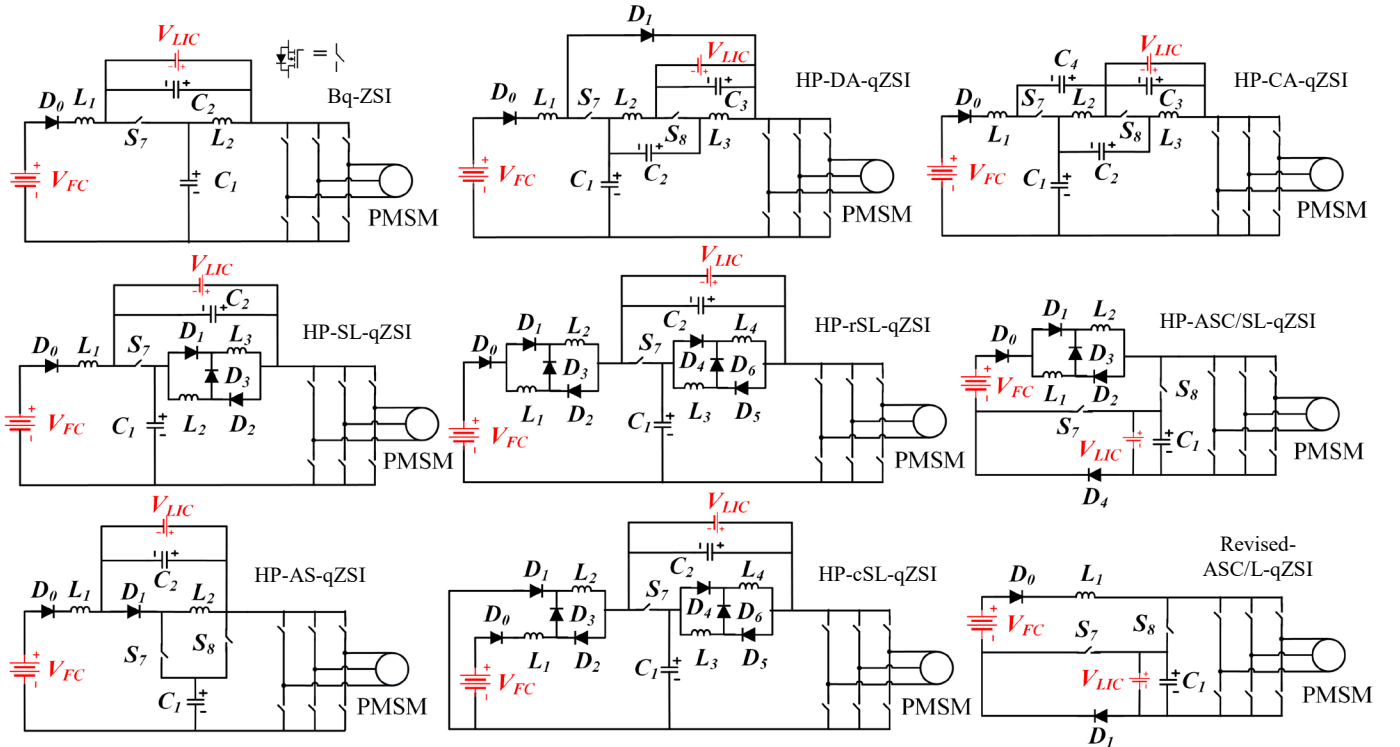


Fig. 2. Schematics of the considered dual-source ZSI topologies in the three-wheel FC-HEV.

characteristics of the FC. There are various criteria that need to be satisfied [26]:

- High efficiency and low power losses are to reduce the fuel consumption and the system size of the powertrain.
- High compactness, low weight and volume are vital owing to the limitation of the utilized FC-HEV internal space.
- High reliability of topologies is essential for commercialization.
- Low input current ripple is required to expand the lifetime of FC stacks.
- Low cost is necessary for commercialization.

After determining the criteria, the hierarchical structure is used to figure out their sub-criteria. It describes how the DMs consider the decisions, and the procedure for assessing the alternatives. As presented in Fig. 6, the established criteria are illustrated in the grey boxes. These criteria can be mixed and evaluated as follows:

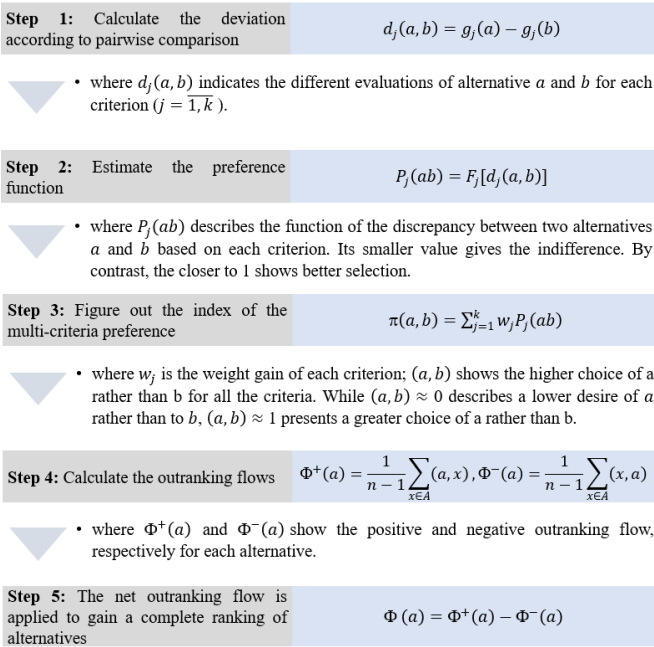


Fig. 5. PROMETHEE process flowchart for complete ranking.

- In order to reach high compactness, low weight, and low volume, it is important to minimize the design values of passive components as well as the number of passive and active components. Moreover, minimizing the power losses is necessary to reduce the heatsink size and volume.
- Reliability of topologies is evaluated by input current ripple, the number of active switches, and common ground (CM GND) structure. The criterion of CM GND is scaled by the five-point Likert, in which the ZSI topology with and without CM GND is indexed by 5, and 1 respectively.
- As each topology has various number of components with different power rating values, the pair-by-pair comparison of all topologies in terms of the voltage and current stresses could not be implemented. Thus, the maximum voltage and current ratings of components at the ZSN are used as the cost criterion.
- Concerning the system cost, it is a complex function, including heatsinks cost, power ratings, and the number of

components as well as their volume and size. It is difficult to quantify exactly the cost of the converters. However, the cost can be minimized by reducing the power losses, the rating of components, and the volume of passive components. Thus, these criteria are mixed by the topology efficiencies, the total passive component values, and the rating of components.

B. Defining the Scenarios for Selecting Z-source Topologies

To provide a wider scope for analyzing the multi-criteria, four different scenarios are considered for implementing the PROMETHEE as:

- **Scenario 1** is considered as the reference for the other scenarios, where the weight gains are figured out from the data.
- **Scenario 2** pays attention to the criteria of the system size, volume, and compactness.
- **Scenario 3** shows the importance of input current ripples.
- **Scenario 4** illustrates the combined criteria of the system size, volume, compactness, and the input current ripples.

In scenario 1, the weight gains are determined based on the entropy method using the data without considering the expert's knowledge [27]. In other scenarios, the weight gains of the important criteria are determined by the expert's knowledge. TABLE III reports the considered weights in each scenario. Based on the presented hierarchical structure in Fig. 6, the weight gain of each criterion is calculated by summing the criterion itself with the other connecting criteria. Each criterion is divided by its number of sub-criteria. For instance, from Fig. 6, the efficiency criterion/topology (W_{eff}) is related to two other criteria: 1) compactness, weight, and volume (W_{com}); 2) cost (W_{cost}). W_{eff} has one sub-criteria while W_{com} and W_{cost} have eight and ten sub-criteria respectively. Thus, the weight gain of the efficiency topology ($W_{total\ eff}$) is determined by:

$$W_{total\ eff} = W_{eff} + \frac{W_{com}}{8} + \frac{W_{cost}}{10} \quad (1)$$

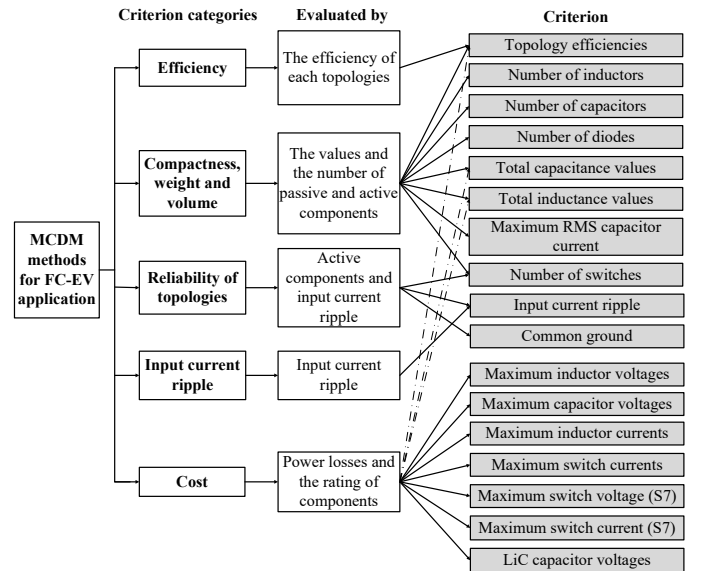


Fig. 6. The hierarchical structure of the primary objectives.

Besides determining the weight gains, selecting the preference function shapes is necessary. It indeed converts the discrepancy in evaluation of alternatives on each criterion into the preference degree, which is restricted from 0 to 1. Among different preference function shapes [21], linear preference function is utilized in this study. It allows the definition of indifference and preference threshold with 2% and 25%, respectively, to keep some choices for alternative *a* versus *b*.

TABLE III
WEIGHT GAINS OF CRITERION CATEGORIES ACCORDING TO SCENARIOS

Scenario	Efficiency	Compact, weight, volume	Reliability	Input current ripple	Cost
S1	-	-	-	-	-
S2	10%	60%	10%	10%	10%
S3	10%	10%	10%	60%	10%
S4	13.33%	30%	13.33%	30%	13.33%

IV. RESULTS AND DISCUSSION

A. Results for Different Scenarios by Using Visual PROMETHEE.

1) Scenario 1 (S1)

Fig. 7 presents the obtained PROMETHEE results for all the scenarios. In S1, the results emphasize that if DMs cannot determine how important the criteria are using the expert’s knowledge, the HP-AS-qZSI and Bq-ZSI are ranked higher than the other topologies, as illustrated in 0. This is mainly because they attain great evaluation values regarding the highest weight gains. These topologies show low input current ripples, low capacitances, and require few diodes in design. Moreover, they impose low LiCs voltage stress. The revised ASC/L-qZSI has also a good rank. However, its high input current ripple and high LiCs voltage stress have led it to the third rank. By contrast, the HP-rSL-qZSI is identified as the lowest-rank topology. Its primary weaknesses are the large number of passive components and the large input current ripple.

2) Scenario 2 (S2)

In S2, the HP-AS-qZSI has achieved better results than the other topologies, followed closely by revised ASC/L-qZSI, as shown in 0. The revised ASC/L-qZSI has fewer passive components and lower capacitance values in design. However, the HP-AS-qZSI compensates for these factors by the lower input current ripple and power losses. The HP-rSL-qZSI still shows the lowest rank among all ZSI topologies.

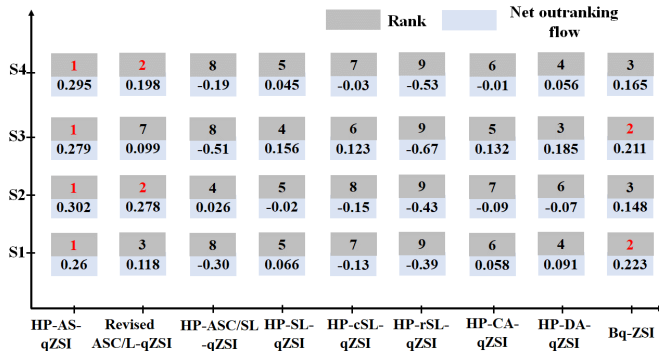


Fig. 7. PROMETHEE results for all scenarios.

3) Scenario 3 (S3)

From Fig. 7, the HP-AS-qZSI and the Bq-ZSI are the best solutions in S3 primarily due to their low input current ripples and high efficiencies. Although the HP-DA-qZSI and HP-SL-qZSI have lower current ripples than these two topologies, the higher number of passive components and lower efficiencies have mainly made them fall behind. In this scenario, the revised ASC/L-qZSI reaches a very low rank compared to other scenarios. This is owing to its large input current ripple. The HP-rSL-qZSI reaches the lowest rank.

4) Scenario 4 (S4)

In S4, which is a combined scenario, the HP-AS-qZSI and the revised ASC/L-qZSI are found to be the best choices mainly due to lower input current ripple and higher compactness. Unlike S3, herein, the revised ASC/L-qZSI has been ranked in a higher position. In fact, it has higher input current ripples. However, its lower power losses and number of passive components makes it a better choice than the Bq-ZSI. The HP-rSL-qZSI has resulted in the lowest rank among all alternatives. The results of the net outranking flows are presented in 0.

B. Comparison of Efficiency and Passive Component Size and Volume.

As pointed out in S1, the HP-AS-qZSI and the Bq-ZSI are the most applicable topologies for the FC-HEV under study as they have achieved a great trade-off among different criteria. In this section, these two topologies are compared with the conventional two-stage inverter (BC-VSI) in terms of efficiency, system size, and volume using different approaches.

1) Efficiency calculation of the selected ZSI topologies

The power losses of qZSI including the power losses in both non-shoot through (NST) state and shoot-through (ST) state is presented for the sinusoidal pulse width modulation scheme with injected 3rd harmonic in [28]. In this study, this analysis is also employed to compare the efficiencies among the three topologies for the simple boost control scheme since this scheme enables to maintain a low FC current ripple.

0 presents the obtained theoretical results regarding the power losses of powertrains using the two selected ZSIs (Bq-ZSI and HP-AS-qZSI) and the conventional BC-VSI. It can be noticed that the HP-AS-qZSI and the Bq-ZSI have achieved lower average losses over the BC-VSI. Thus, using these two topologies leads to higher average efficiency over the usage of the BC-VSI. However, comparing the efficiency of the FC/LiC

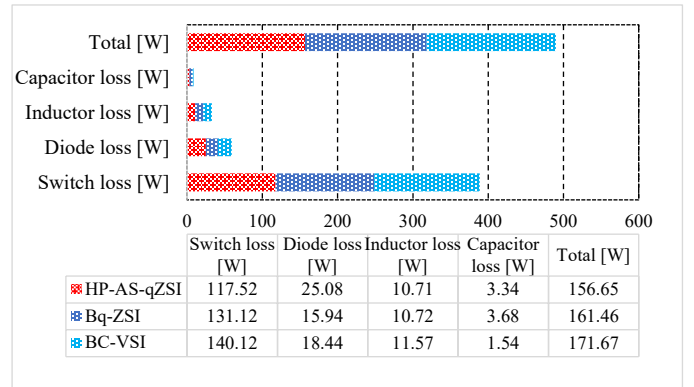


Fig. 8. Calculated average losses of the topologies under the same driving cycle with single input source of 60 V.

topologies are a difficult task because the current of the hybrid ESS is determined by the EMS [29]. Hence, further attention, as explained in this section, is required to realize the efficiency improvement in these topologies.

To evaluate the efficiency enhancement of the ZSI topologies, an effective approach is to calculate the decreased average ST current of the power switching device in each leg of the inverter part. This method has already been utilized for a Bq-ZSI in a hybrid SC/BAT powertrain configuration [13]. The same approach is also applied to the ZSIs of the hybrid FC/LiC configuration in this work.

The HESS HP-AS-qZSI operations during continuous conduction mode (CCM) in both the NST and ST states are illustrated in Fig. 9a, Fig. 9b, respectively. In this CCM, the power switching device S_8 will not conduct, and there is just current flowing through its freewheeling diode D_8 .

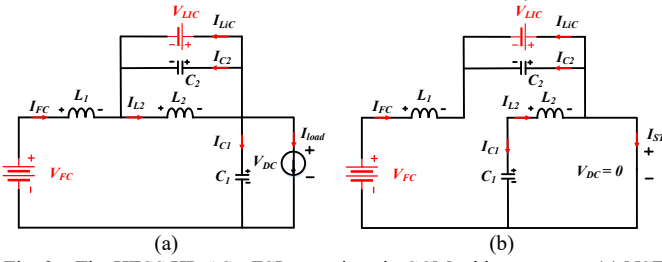


Fig. 9. The HESS HP-AS-qZSI operations in CCM with two states. (a) NST state, (b) ST state.

During the NST state in Fig. 9a, the switching device S_7 is switched off, whereas the diodes (D_1, D_8) are conducted. The inductors (L_1, L_2) discharge their stored energies into the capacitors (C_1, C_2) and the load. The dynamic equations in this state are determined by:

$$\begin{cases} L_1 \frac{di_{FC}}{dt} = v_{FC} + v_{C2} - v_{C1} \\ L_2 \frac{di_{L2}}{dt} = -v_{C2} \\ C_1 \frac{du_{C1}}{dt} = i_{FC} - i_{load} \\ C_2 \frac{du_{C2}}{dt} = i_{L2} - i_{load} - i_{LIC} \end{cases} \quad (2)$$

In the ST state in Fig. 9b, the dc-link is shorted by the upper and lower switches of the phase legs inverter. The S_7 is turned on, and the diodes (D_1, D_8) are in blocked states. The two inductors (L_1, L_2) are charged, while the two capacitors (C_1, C_2) transfer their powers during this state. The dynamic equations are shown as (3):

$$\begin{cases} L_1 \frac{di_{FC}}{dt} = v_{FC} + v_{C2} \\ L_2 \frac{di_{L2}}{dt} = v_{C1} \\ C_1 \frac{du_{C1}}{dt} = -i_{L2} = -i_{st} + i_{FC} \\ C_2 \frac{du_{C2}}{dt} = -i_{L1} - i_{LIC} \end{cases} \quad (3)$$

By employing the voltage/ampere-second balance principle to the capacitors and the inductors over one switching period, the ST and LiC currents are derived as (4):

$$\begin{cases} B = V_{C1} = \frac{1 - D_{st}}{1 - 3D_{st} + D_{st}^2} v_{FC} \\ V_{LIC} = V_{C2} = \frac{D_{st}}{1 - 3D_{st} + D_{st}^2} v_{FC} \\ I_{ST} = I_{L2} + I_{FC} \\ I_{LIC} = I_{L2} - I_{FC} \end{cases} \quad (4)$$

where D_{st} represents the shoot-through duty cycle and B is the boost factor.

From (4), the total ST current in the inverter parts of the Bq-ZSI and HP-AS-qZSI can be simply estimated by (5):

$$I_{ST} = 2I_{FC} + I_{LIC} \quad (5)$$

where I_{FC} and I_{LIC} are the FC and LiC current, respectively.

The average ST current of the switching devices in single leg is:

$$I_{ST_AVG} = \frac{2}{3}I_{FC} + \frac{1}{3}I_{LIC} \quad (6)$$

I_{ST_AVG} can be rewritten as follows:

$$I_{ST_AVG} = - \left[\left(2 + \frac{V_{FC}}{V_{LIC}} \right) \cdot \frac{P_o}{3V_{FC}} \right] \cdot \frac{P_{LIC}}{P_o} + \frac{2P_o}{3V_{FC}} \quad (7)$$

where P_o is the PMSM power, P_{LIC} is the LiC power, V_{FC} is the FC voltage and V_{LIC} is the LiC voltage. By changing LiC power from zero to the PMSM power, the I_{ST_AVG} range can be realized as follows:

$$-\frac{V_{FC}}{V_{LIC}} \cdot \frac{P_o}{3V_{FC}} \leq I_{ST_AVG} \leq \frac{2P_o}{3V_{FC}} \quad (8)$$

If $\frac{V_{FC}}{V_{LIC}} \leq 2$, it is straightforward to obtain:

$$-\frac{2P_o}{3V_{FC}} \leq I_{ST_AVG} \leq \frac{2P_o}{3V_{FC}} \quad (9)$$

From (7), the Bq-ZSI and HP-AS-qZSI using single FC source could be considered as the specific scenario in which the LiC power is equal to zero. Thus, their I_{ST_AVG} can be expressed as follows:

$$I_{ST_AVG} = \frac{2P_o}{3V_{FC}} \quad (10)$$

Based on (9) and (10), it is well understood that in the ST state, the amplitudes of I_{ST_AVG} are decreased in the Bq-ZSI and HP-AS-qZSI of the FC/LiC configuration. This leads to reduced switching and conduction losses of the IGBTs in the inverter part, compared to those losses in the single-input FC source-based ZSI topologies.

2) Comparison of passive components size and volume

The overall stored energy in topologies is employed as a criterion to compare the passive components size and volume of the Bq-ZSI and the conventional inverter in [30]. This energy is composed of the magnetic energy (W_{L_ZSI}) and the electrostatic energy (W_{C_ZSI}) of the selected ZSI topologies, calculated by (11) and (12):

$$W_{L_ZSI} = \frac{1}{2}L_1 i_{L1}^2 + \frac{1}{2}L_2 i_{L2}^2 \quad (11)$$

$$W_{C_ZSI} = \frac{1}{2}C_1 v_{C1}^2 + \frac{1}{2}C_2 v_{C2}^2 \quad (12)$$

where $L_{1,2}$ and $C_{1,2}$ are the inductances and capacitances of the Bq-ZSI and HP-AS-qZSI, respectively.

As pointed out, the higher stored energy leads to increased volume and cost. The comparison of the stored energy by the three topologies is presented in Fig. 10. As is seen, the

conventional topology shows the highest stored energy for the two FC voltages (60 V and 48 V) followed by Bq-ZSI and HP-AS-qZSI respectively. Thus, the Bq-ZSI and HP-AS-qZSI require smaller passive elements than the conventional one.

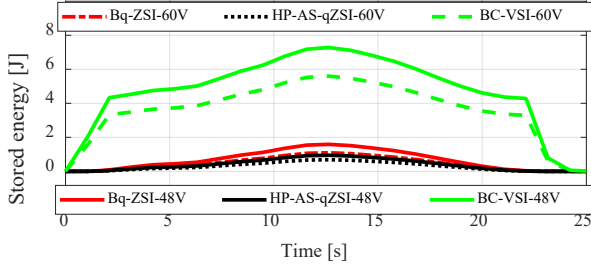


Fig. 10. Stored energy in the three topologies under the studied driving cycle with two different FC voltages (48V and 60V).

C. HIL Validation of the first Two-Ranked Topologies.

The signal HIL simulation based on OP4510 from OpalRT is conducted to verify the real-time operation of the two first ranked ZSI topologies in S1 and the conventional two-stage inverter based on the semi-active FC/LiC configuration using the presented parameters in TABLE I. These three topologies are firstly implemented on the OP4510 FPGA-based Electric Hardware Solver. The TMS320F28335 experimenter kit is then utilized to execute the control algorithm as presented in Fig. 3.

Fig. 11 shows the PMSM torque and speed waveforms of the three topologies obtained from the experimental HIL. It can be observed that the speeds follow well the references, while the torques demonstrate small ripples. The FC and LiC current waveforms of the three topologies are illustrated in Fig. 12. From time 0s to 1.2s and 23s to 25s, the PMSM powers are equal to zero. So, all the FC powers are used to charge the LiCs. However, LiC currents of the selected ZSI topologies are higher than that of the conventional one because of the lower level of voltage used in their LiCs. From 5s to 20s, both LiC and FC supply power to the PMSM. Moreover, the FC current ripples of the selected topologies are slightly different than that of the conventional one due to their lower inductance values. Fig. 13 presents the experimental voltage waveforms of the LiC, FC, and the DC link. From this figure, the DC link voltage of the conventional configuration is more stable than those of the Bq-ZSI and the HP-AS-qZSI as its LiC is placed in parallel with the DC link capacitor. The PMSM current experimental results of the Bq-ZSI and HP-AS-qZSI are illustrated in Fig. 14.

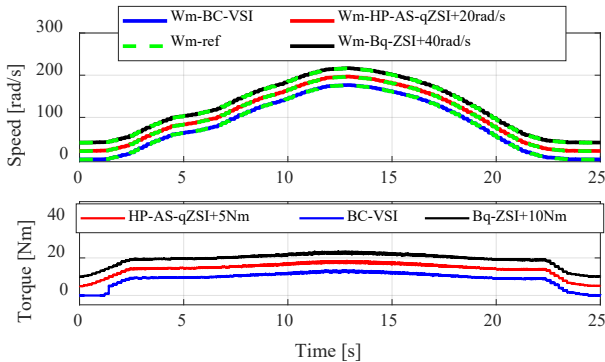


Fig. 11. Experimental results for speed and torque of the motor.

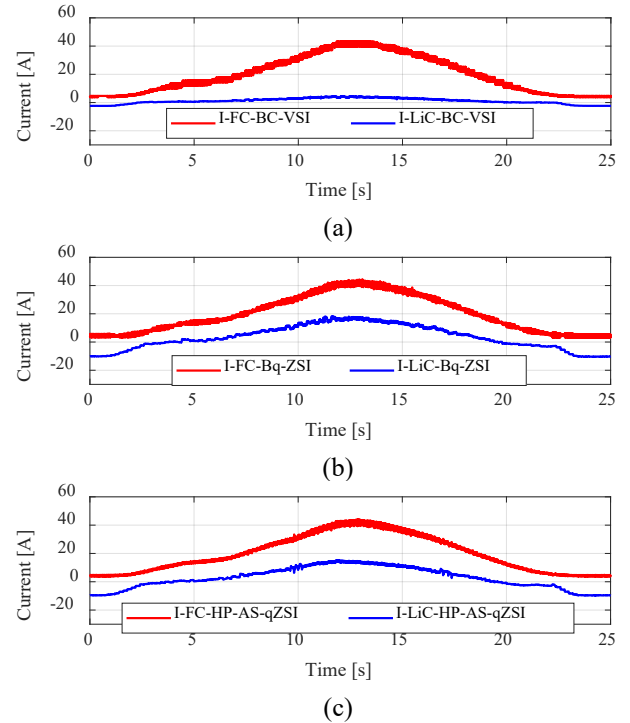


Fig. 12. Experimental results of FC and LiC currents for the studied FC-HEV, (a) BC-VSI, (b) Bq-ZSI and (c) HP-AS-qZSI.

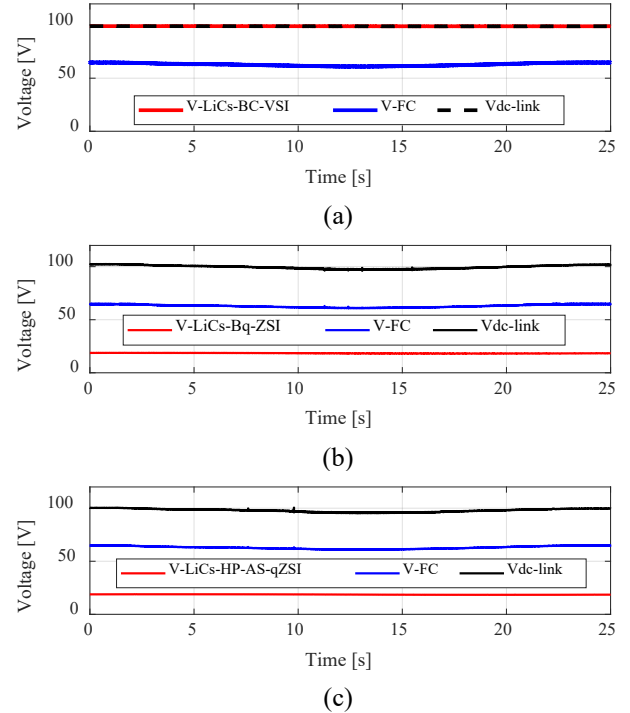


Fig. 13. The experimental voltage of the LiC, FC, and the DC link, (a) BC-VSI, (b) Bq-ZSI and (c) HP-AS-qZSI.

According to this figure, the PMSM currents show good control qualities by these topologies. Based on these results, it can be concluded that controlling the three-wheel FCEV-based PMSM has been properly performed by these three topologies under the studied driving cycle.

Regarding the efficiency, the experimental results are presented in Fig. 15. The average efficiencies of the HESS HP-AS-qZSI and the HESS Bq-ZSI are 73.13% and

71.04%, respectively, while that of the HESS conventional one is 69.06%.

From Fig. 15, the system efficiency of the HESS ZSI topologies is significantly increased from 1.98% to 4.07% compared to that of the HESS conventional one.

Although the HP-AS-qZSI has more active switches and diodes than the Bq-ZSI, its design value of the capacitance is much lower than that of the Bq-ZSI. Furthermore, their voltage stresses on LiCs are lightly different in Fig. 13, thus the same sizes of the LiCs are used. It is apparently understood that using the HESS FC/LiCs HP-AS-qZSI would lead to smaller system size and volume, and higher compactness than the HESS FC/LiCs Bq-ZSI. This is also demonstrated by the scenario 2 evaluation.

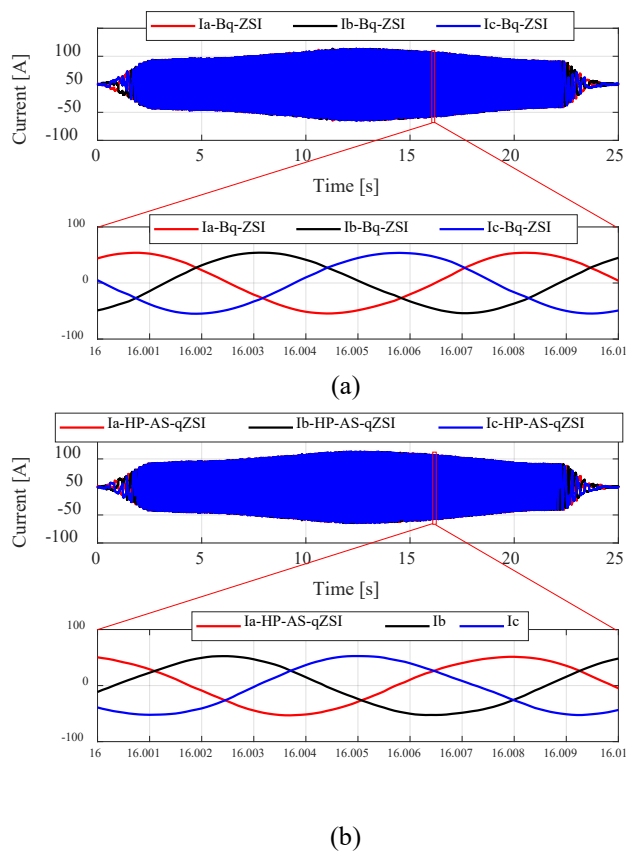


Fig. 14. PMSM current experimental results of the selected ZSI topologies, (a) Bq-ZSI and (b) HP-AS-qZSI.

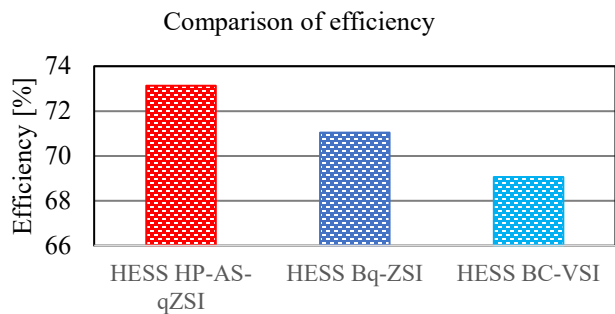


Fig. 15. Efficiencies experimental results.

V. CONCLUSION

This paper introduces a MCDM approach to rank dual-source ZSI topologies for a three-wheel FC-HEV. The ZSI topologies are evaluated in terms of five criteria, namely efficiency, compactness (weight and volume), reliability, input current ripple, and cost under four different scenarios, including standard, compactness, input current ripple, and combination of compactness and current ripples. Consequently, the most suitable ZSI topologies are realized to enhance the performance of the FC-HEV. In this regard, PROMETTEE method is employed as the decision-making aid tool. In the standard scenario, the HP-AS-qZSI and Bq-ZSI seem to be the best options. In terms of compactness, weight, and volume factors, the HP-AS-qZSI is considered as the best topology, followed by the revised ASC/L-qZSI. Regarding the input current ripple scenario, the HP-AS-qZSI and Bq-ZSI achieve better results than the others. In the last scenario, the HP-AS-qZSI and the revised ASC/L-Bq-ZSI are found as the best topologies. Based on scenario 1, the HP-AS-qZSI and the Bq-ZSI are the most suitable ZSI topologies for the studied FC-HEV as they have achieved a great trade-off among multiple criteria. Moreover, the comparative results and the HIL experimental results of these two highest-ranked topologies have demonstrated that the HP-AS-qZSI and the Bq-ZSI have higher efficiency, lower input current ripple, and better system size and volume, compared to the conventional two-stage inverter.

These results indicate that the systematic methodology proposed in this study can also be utilized in supporting decision-makers to choose appropriate HESS ZSI topologies for improving the performance of various FC-HEVs. Furthermore, the HP-AS-qZSI and the Bq-ZSI will be practicable alternatives to replace the conventional and used two-stage inverter in the FC-HEV as more effective solutions in terms of compactness, size and volume, and performance. For future work to broaden this study, a robust control algorithm will be proposed to manage these selected two HESS FC/LiCs ZSI topologies for the particular application of a 3-wheel EV.

REFERENCES

- [1] M. W. Beraki, J. P. F. Trovao, M. S. Perdigao, and M. R. Dubois, "Variable Inductor Based Bidirectional DC-DC Converter for Electric Vehicles," *IEEE Trans Veh Technol*, vol. 66, no. 10, pp. 8764–8772, 2017.
- [2] R. Ghaderi, M. Kandidayeni, M. Soleymani, L. Boulon, and J. P. F. Trovao, "Online Health-Conscious Energy Management Strategy for a Hybrid Multi-Stack Fuel Cell Vehicle Based on Game Theory," *IEEE Trans Veh Technol*, vol. 9545, no. c, pp. 1–1, 2022.
- [3] Q. I. Grid-tie and P. P. Generation, "Control System Design of Battery-Assisted Quasi-Z-Source Inverter for Grid-Tie Photovoltaic Power Generation," *EEE Transactions on Sustainable Energy*, vol. 4, no. 4, pp. 994–1001, 2013.
- [4] M. K. Nguyen, Y. C. Lim, and S. J. Park, "Improved trans-Z-source inverter with continuous input current and boost inversion capability," *IEEE Trans Power Electron*, vol. 28, no. 10, pp. 4500–4510, 2013.
- [5] S. M. Dehghan, M. Mohamadian, and A. Yazdian, "Hybrid electric vehicle based on bidirectional Z-source nine-switch inverter," *IEEE Trans Veh Technol*, vol. 59, no. 6, pp. 2641–2653, 2010.
- [6] F. Guo, L. Fu, C. H. Lin, C. Li, W. Choi, and J. Wang, "Development of an 85-kW bidirectional quasi-Z-source inverter with DC-link feed-

- forward compensation for electric vehicle applications,” *IEEE Trans Power Electron*, vol. 28, no. 12, pp. 5477–5488, 2013.
- [7] S. Dong and Q. Zhang, “CCM and DCM analysis of ASC-qZSI,” *IET Power Electronics*, vol. 12, no. 8, pp. 2049–2057, 2019.
- [8] A. V. Ho, T. W. Chun, H. H. Lee, and H. G. Kim, “Active switched quasi-Z-source inverter with high-boost ability for low-voltage renewable energy sources,” *5th International Conference on Clean Electrical Power: Renewable Energy Resources Impact, ICCEP 2015*, pp. 627–632, 2015.
- [9] A. V. Ho, T. W. Chun, and H. G. Kim, “Extended boost active-switched-capacitor/switched-inductor quasi-Z-source inverters,” *IEEE Trans Power Electron*, vol. 30, no. 10, pp. 5681–5690, 2015.
- [10] M. Nguyen, Y. Lim, and G. Cho, “Switched-Inductor Quasi-Z-Source Inverter,” *IEEE Trans Power Electron*, vol. 26, no. 11, pp. 3183–3191, 2011.
- [11] M. K. Nguyen, Y. C. Lim, and J. H. Choi, “Two switched-inductor quasi-Z-source inverters,” *IET Power Electronics*, vol. 5, no. 7, pp. 1017–1025, 2012.
- [12] C. J. Gajanayake, F. L. Luo, H. Gooi, P. L. So, and L. K. Siow, “Extended-Boost Z -Source Inverters,” *IEEE Trans Power Electron*, vol. 25, no. 10, pp. 2642–2652, 2010.
- [13] S. Hu, Z. Liang, D. Fan, and X. He, “Hybrid Ultracapacitor-Battery Energy Storage System Based on Quasi-Z-source Topology and Enhanced Frequency Dividing Coordinated Control for EV,” *IEEE Trans Power Electron*, vol. 31, no. 11, pp. 7598–7610, 2016.
- [14] S. Hu, Z. Liang, and X. He, “Ultracapacitor-Battery Hybrid Energy Storage System Based on the Asymmetric Bidirectional Z-Source Topology for EV,” *IEEE Trans Power Electron*, vol. 31, no. 11, pp. 7489–7498, 2016, doi: 10.1109/TPEL.2015.2493528.
- [15] F. Z. Peng, M. Shen, and K. Holland, “Application of Z-source inverter for traction drive of fuel cell-battery hybrid electric vehicles,” *IEEE Trans Power Electron*, vol. 22, no. 3, pp. 1054–1061, 2007.
- [16] D. Mande, J. P. F. Trovão, M. C. Ta, and T. van Do, “Dual-Source Bidirectional Quasi-Z-Source Inverter Development for Off-Road Electric Vehicles,” *World Electric Vehicle Journal*, vol. 13, no. 9, 2022.
- [17] K. C. Omran and A. Mosallanejad, “SMES/battery hybrid energy storage system based on bidirectional Z-source inverter for electric vehicles,” *IET Electrical Systems in Transportation*, vol. 8, no. 4, pp. 215–220, 2018.
- [18] S. Hu, Z. Liang, and X. He, “Research on the Dynamic Characteristics and Regulation Method of the Energy Stored Quasi-Z-Source Inverter System,” *IEEE Transactions on Industrial Electronics*, vol. 67, no. 6, pp. 4590–4599, 2020.
- [19] M. Hamurcu and T. Eren, “Electric bus selection with multicriteria decision analysis for green transportation,” *Sustainability (Switzerland)*, vol. 12, no. 7, 2020.
- [20] E. U. Ergul, A. Yildiz, and L. Ugur, “The Best Vehicle Engine System Selection using VIKOR and TOPSIS Methods,” *International Conference of Engineering & natural sciences*, no. March 2017, pp. 1217–1223, 2016.
- [21] J. A. Manzolli, J. P. Trovão, and C. Henggeler Antunes, “Scenario-Based Multi-criteria decision analysis for rapid transit systems implementation in an urban context,” *eTransportation*, vol. 7, no. 2590–1168, p. 100101, 2021.
- [22] Y. Wu, M. Yang, H. Zhang, K. Chen, and Y. Wang, “Optimal site selection of electric vehicle charging stations based on a cloud model and the PROMETHEE method,” *Energies (Basel)*, vol. 9, no. 3, pp. 1–20, 2016.
- [23] A. Macías, M. Kandidayeni, L. Boulon, and J. Trovão, “Passive and Active Coupling Comparison of Fuel Cell and Supercapacitor for a Three-Wheel Electric Vehicle,” *Fuel Cells*, vol. 20, no. 3, pp. 351–361, 2020.
- [24] J. P. F. Trovao, M. A. Roux, E. Menard, and M. R. Dubois, “Energy- and power-split management of dual energy storage system for a three-wheel electric vehicle,” *IEEE Trans Veh Technol*, vol. 66, no. 7, pp. 5540–5550, 2017.
- [25] J.-P. Brans and Y. De Smet, *Chapter 1 PROMETHEE Methods*, no. July 2018. 2016. doi: 10.1007/978-1-4939-3094-4.
- [26] H. Wang, A. Gaillard, and D. Hissel, “A review of DC/DC converter-based electrochemical impedance spectroscopy for fuel cell electric vehicles,” *Renew Energy*, vol. 141, no. 0960–1481, pp. 124–138, 2019.
- [27] A. Jeklin, *Decision Making in the Manufacturing Environment Using Graph Theory and Fuzzy Multiple Attribute Decision Making Methods*, no. July. 2016.
- [28] I. Grgić, D. Vukadinović, M. Bašić, and M. Bubalo, “Calculation of semiconductor power losses of a three-phase quasi-Z-source inverter,” *Electronics (Switzerland)*, vol. 9, no. 10, pp. 1–20, 2020.
- [29] B. H. Nguyen, R. German, J. P. F. Trovao, and A. Bouscayrol, “Real-time energy management of battery/supercapacitor electric vehicles based on an adaptation of pontryagin’s minimum principle,” *IEEE Trans Veh Technol*, vol. 68, no. 1, pp. 203–212, 2019.
- [30] A. Battiston, J.-P. Martin, E.-H. Miliani, B. Nahid-Mobarakeh, S. Pierfederici, and F. Meibody-Tabar, “Comparison Criteria for Electric Traction System Using Z-Source/Quasi Z-Source Inverter and Conventional Architectures,” *IEEE J Emerg Sel Top Power Electron*, vol. 2, no. 3, pp. 467–476, 2014.

APPENDIX

A. Data for Implementing the PROMETHEE.

TABLE IV
DATA FROM OFFLINE MATLAB/SIMULINK SIMULATION FOR IMPLEMENTING THE PROMETHEE METHOD

Alternatives	Efficiency (%)	Input current ripple (%)	No. S	No. L	No. C	No. D	Total C (mF)	Total L (μ H)	Vc max (V)	IL max (A)	Ipn max (A)	Vs7 max (V)	Is7 max (A)	VLiC (V)	IC RMS	VL max	CM GND
HP-AS-qZSI	74.67	10.61	8	2	2	2	4.1232	162.634	101	50.5	98.25	87.5	55.2	18.3	33.1	87.4	5
Revised ASC/L-qZSI	74.04	21.22	8	1	1	1	1.0422	192	101	46.8	68.5	101.6	46.8	100.8	19.6	165.6	1
HP-ASC/SL-qZSI	70.86	75	8	2	1	5	1.7498	173.657	101	45.1	90.05	100	90.1	101.1	24.6	163.6	1
HP-SL-qZSI	66.58	9.02	7	2	2	4	4.712	215.335	78	44.2	130	100	86.8	23.5	42.9	87.5	5
HP-cSL-qZSI	64.64	7.81	7	4	2	7	7.4572	192	79	45.8	176	100	89.5	22	43.8	85.1	5
HP-rSL-qZSI	62.58	72.86	7	4	2	7	6.2261	220.689	83	57	200	100	100	18.5	50.1	85.4	5
HP-CA-qZSI	65.52	7.66	8	3	4	1	20.2871	192	77.2	59	142.8	101.5	62.5	12.3	46	89.2	5
HP-DA-qZSI	70.94	5.44	7	3	3	2	13.7447	222.069	74	57.1	132.1	72	89	13.3	42.8	85.3	5
Bq-ZSI	71.43	9.52	7	2	2	1	5.4167	192	83	57.5	100.8	100.4	100.9	18.5	35.5	82.6	5



Thang Van Do (Student Member, IEEE) was born in Hai Phong, Viet Nam, in 1994. He received his B.S. degree from Ha Noi University of Science and Technology, Ha Noi, Viet Nam, in 2017, in control and automation engineering, the M.S. degree in electrical engineering from Changwon National University, Changwon, South Korea, in 2019. He is currently pursuing the Ph.D. degree in electrical engineering with University of Sherbrooke, Sherbrooke, Canada. His research interests include power electronics, renewable energy, and electric vehicles.



Mohsen Kandidayeni (Member, IEEE) was born in Tehran, Iran, in 1989. He received the B.S. degree in mechanical engineering in 2011, the master's degree (Hons.) in mechatronics from Arak University, Iran, in 2014, and the Ph.D. degree (Hons.) in electrical engineering from the University of Quebec at Trois-Rivières (UQTR), QC, Canada, in 2020. His educational journey has spanned through different paths. In 2016, he joined the Hydrogen Research Institute, UQTR. He is currently a Post-Doctoral

Researcher with the electric-Transport, Energy Storage and Conversion Lab (e-TEESC), *Université de Sherbrooke*, and a Research Assistant Member with the Hydrogen Research Institute, UQTR. He has been actively involved in conducting research through authoring, coauthoring, and reviewing several articles in different prestigious scientific journals and also participating in various international conferences. His research interest includes energy-related topics, such as hybrid electric vehicles, fuel cell systems, energy management, multiphysics systems, modeling, and control. Moreover, he has been a recipient of several awards/honors during his educational path, such as the Doctoral Scholarship from the *Fonds de recherche du Québec—Nature et technologies* (FRQNT), the Post-Doctoral Scholarship from FRQNT, the Excellence Student Grant from UQTR, and the Third Prize in Energy Research Challenge from the Quebec Ministry of Energy and Natural Resources.



João Pedro F. Trovão (Senior Member, IEEE) received the M.Sc. and Ph.D. degrees in electrical engineering from the University of Coimbra, Coimbra, Portugal, in 2004 and 2013, respectively. From 2000 to 2014, he was a Teaching Assistant and an Assistant Professor with the Polytechnic Institute of Coimbra—Coimbra Institute of Engineering (IPC—ISEC), Portugal. Since 2014, he has been a Professor with the Department of Electrical Engineering and Computer Engineering, University

of Sherbrooke, Sherbrooke, QC, Canada, where he currently holds the Canadian research chair position in efficient electric vehicles with the Hybridized Energy Storage Systems. He is also the Founding Member and the Director of the electric-Transport, Energy Storage and Conversion (e-TEESC) Lab, University of Sherbrooke. He is the author/coauthor of over 180 journal articles and conference papers. His research interests cover the areas of electric vehicles, hybridized energy storage systems, energy management, and rotating electrical machines. He was the General Chair of the 2018 IEEE Vehicle Power and Propulsion Conference, Chicago, IL, USA. He was a Guest Editor for the Special Issue of *IET Electrical Systems in Transportation* on energy storage and electric power sub-systems for advanced vehicles and the Special Issue of IEEE TRANSACTIONS ON VEHICULAR TECHNOLOGY on electric powertrains for future vehicles and on advanced vehicle power propulsion systems. He is also a Senior Editor of the automotive electronics topic of the *IEEE Vehicular Technology Magazine*.



Loïc Boulon (Senior Member, IEEE) received the master's degree in electrical and automatic control engineering from the University of Lille, France, in 2006, and the Ph.D. degree in electrical engineering from the University of Franche-Comté, France. Since 2010, he has been a Professor with UQTR, where he has been a Full Professor since 2016. Since 2019, he has been the Deputy Director of the Hydrogen Research Institute. His work deals with modeling, control, and energy management of multiphysics systems. He has published more than 120 scientific

articles in peer-reviewed international journals and international conferences

and given over 35 invited conferences all over the world. His research interests include hybrid electric vehicles and energy and power sources, such as fuel cell systems, batteries, and ultracapacitors. In 2015, he was the General Chair of the IEEE-Vehicular Power and Propulsion Conference in Montréal, QC, Canada. He is also the VP of Motor Vehicles of the IEEE Vehicular Technology Society and the Founder of the International Summer School on Energetic Efficiency of Connected Vehicles and the IEEE VTS Motor Vehicle Challenge. He is also the holder of the Canada research chair position of energy sources for the vehicles of the future.